Article:

Mo, P-Q, Marshall, AM and Yu, H-S (2015) Centrifuge modelling of cone penetration tests in layered soils. Géotechnique, 65 (6). pp. 468-481. ISSN 0016-8505

https://doi.org/10.1680/geot.14.P.176

Centrifuge modelling of cone penetration tests in layered soils

Pin-Qiang Mo, Research Fellow
corresponding author
email Pinqiang.Mo@nottingham.ac.uk
tel 0115 951 4102
Faculty of Engineering, University of Nottingham
University Park, Nottingham NG7 2RD

Alec M. Marshall, Lecturer
Faculty of Engineering, University of Nottingham
University Park, Nottingham NG7 2RD

Hai-Sui Yu, Professor
Faculty of Engineering, University of Nottingham
University Park, Nottingham NG7 2RD

revised on January 15, 2015
approx 5000 words
16 Figures
2 Tables

Abstract

Penetration problems are important in many areas of geotechnical engineering, such as the prediction of pile capacity and interpretation of in-situ test data. **[Reply 3-1] The cone penetration test is a proven method for evaluating soil properties, yet relatively little research has been conducted to understand the effect of soil layering on penetrometer readings. This paper focuses on the penetration of a probe within layered soils and investigates the layered soil effects on both penetration resistance and soil deformation.** A series of centrifuge tests was performed in layered configurations of silica sand with varying relative density in a 180° axisymmetric model container. The tests allowed for the use of a half-probe for observation of the induced soil deformation through a Perspex window **[Reply 3-2] as well as a full-probe for measurement of penetration resistance within the central area of the container**. The variations of penetration resistance and soil deformation characteristics as they relate to penetration depth, soil density, and soil layering are examined. The results of deformation are also compared with previous experimental data to examine the effect of the axisymmetric condition. The effects of soil layering on both resistance and soil deformation are shown to be dependent on the relative properties between soil layers.

Keywords: cone penetration test, layered soils, centrifuge modelling.

List of notations provided at end of paper.

1 Introduction

It is increasingly important for geotechnical engineers to cost-effectively determine engineering properties of soil using in-situ test methods, which avoid the difficulties in retrieving undisturbed samples. The cone penetration test (CPT) is one of the most versatile devices for in-situ soil testing and has been widely used in geotechnical engineering practice. The CPT can provide reliable and repeatable data which can be used to evaluate soil properties and to delineate between layers of different soil types and states (IRTP, 1994). The analogues between a penetrometer and a displacement pile in both geometry and installation method make the study of penetration problems relevant to a wide range of foundation problems. CPT-based design methods have been developed for piles (Jardine and Chow, 1996; Lehane et al., 2005; White and Bolton, 2005) and for the evaluation of liquefaction potential of soils (Robertson, 1982; Tseng, 1989; Moss et al., 2006).

The interpretation of CPT data tends to rely on empirical relationships, of which many have been developed over the years for soil identification and classification. Numerical modelling has many advantages compared to empirical methods and can provide insights into the relationship between soil characteristics and probe response. However analysis of penetration problems using numerical models is difficult due to the large strains that are induced within the ground in the localised area around the probe. The detailed soil stress/strain history associated with pile/probe installation and the relationship to the distribution of the load on the probe are still not well understood. A review of the methods that have been developed for CPT data analysis was provided by Yu and Mitchell (1998).

One of the complicating factors in the interpretation of CPT data (e.g. cone tip resistance, q_c , and sleeve friction, f_s) is that readings are influenced not only by the soil at the location of the cone tip but also by the soil within an influence zone extending some distance beneath and above the tip. There has been relatively little research done on the effect of soil layering on CPT measurements. A small number of experiments have been carried out that provide observations of the transition of penetration resistance through layered soils (e.g. Treadwell, 1976; Silva and Bolton, 2004; Xu, 2007). There have also been some numerical simulations conducted for the analysis of layered effects and the definition of the influence zones around soil interfaces (e.g. van den Berg et al., 1996; Ahmadi and Robertson, 2005; Xu and Lehane, 2008; Walker and Yu, 2010). The first analytical solution for penetration in layered soils was proposed by Vreugdenhil et al. (1994), which is an approximate solution for simple linear-elastic media. Elastic-plastic solutions for expanding cavities embedded in two different cohesive-frictional materials were proposed by Mo et al. (2014*b*), which were shown to provide an effective method for the interpretation of CPT data in layered soils in Mo et al. (2014*a*).

Geotechnical centrifuge testing provides an effective experimental method for the study of penetration problems and allows replication of full-scale stress levels and gradients within small-scale models. Previous CPT-based centrifuge tests have provided useful information relating to the effects of boundaries, stress level, and grain size ratio (Lee, 1990; Bolton et al., 1993; Gui et al., 1998). A new test methodology for CPT modelling within a geotechnical centrifuge has been developed in this research, using a 180° axisymmetric model so that image-based methods (White et al., 2003) could be used to acquire sub-surface displacements around a cylindrical probe. The decision to use an axisymmetric model, rather than a fully 3D or plane-strain one, was based on the desire to see and measure the mechanisms of deformation that occur within the soils around a representative cylindrical probe. The axisymmetric condition provides this ability, but involves additional experimental complications which are discussed in the paper.

This paper presents an experimental study of the CPT response in layered soils using geotechnical centrifuge testing. The aim of the work is to investigate the relationship between layered soil properties and penetrometer response. A full description of the experimental equipment and methodology is first provided. This is followed by experimental results **including the transition of penetration resistance ratio to illustrate the effect of layered soil properties on penetrometer response (2-layer and 3-layer profiles are considered), as well as comparison with previous numerical and analytical studies.** Soil displacement profiles and trajectories as well as strain paths are then provided to illustrate the observed penetration mechanisms in both uniform and layered soils. The paper ends with an appropriate set of conclusions.

2 Centrifuge Modelling Methodology

2.1 Experimental apparatus

The centrifuge tests focused on the use of an axisymmetric model (rather than plane-strain) in order to obtain measurements of sub-surface displacements yet still be consistent with the geometric and stress/strain conditions around a cylindrical penetrometer. The centrifuge container, illustrated in Fig. 1, has an inner diameter (D) of $500\,mm$ and a $75\,mm$ thick transparent Perspex wall installed at the centre of the container as a plane of symmetry. A vertical load actuator capable of providing a maximum load of $10\,kN$ was used to drive probes into the soil to a maximum displacement of $220\,mm$. **[Reply 3-15] Sub-surface soil displacements were measured using the particle image velocimetry (PIV) and photogrammetry method of White et al. (2003) on images obtained from two Canon Powershot G10 digital cameras mounted in front of the Perspex wall.** The PSRemote Multi-Camera software was used to simultaneously capture images from the two cameras every 5 seconds. An array of 16 control points was painted onto the Perspex window within each camera's field-of-view (FOV) for use within the White et al. (2003) geoPIV analysis method.

[Fig. 1 about here.]

2.2 Model penetrometers

Aluminium alloy probes with a 12 mm diameter (B), a smooth un-coated shaft, and an apex angle of 60 ° were used for the centrifuge tests (Fig. 2). For the half-probe, the ratio of the container to the probe diameter ($D/B = 42$) and the ratio of the probe diameter to the mean grain size of the soil ($B/d_{50} = 86$) were greater than that suggested by Gui et al. (1998) in order to reduce the boundary and grain size effects. Full-probe tests were also performed in the same samples to provide a more conventional (and reliable) measure of penetration resistance away from the container boundaries. **[Reply 3-16] The distance from the full-probe to the container boundaries was just under the $10B = 127mm$ value (see Fig. 1b) recommended by Gui et al. (1998) to limit boundary effects on penetrometer readings.**

Attempts have been made by previous researchers to accurately model half-probes in the centrifuge (Liu, 2010; Marshall and Mair, 2011). However, any intrusion of sand particles between the half-probe and the window forces the probe to deviate from the window, causing bending of the probe and the inability to track its position using image analysis. This problem, which is not such an issue for plane-strain tests (e.g. White, 2002), is one of the main challenges when using a 180 ° axisymmetric model for these types of tests. In order to maintain contact between the probe and the window in this project, a new method was developed which used a guide bar and channel system (Fig. 2a). The guide bar was connected to the half-probe along its length so that the separation between the bar and the probe was fixed. During testing, the probe was pushed with its flat edge down the plane of symmetry of the Perspex wall and the bar slid into the channel (8 mm wide by 8 mm depth) which was fixed within the Perspex wall such that it was flush with the plane of symmetry. This method ensured that the probe followed the exact same vertical path in each test and prevented soil from getting between the probe and the Perspex. To minimise friction along the back of the probe and the guide bar, the contacting surfaces were coated with silicon grease. The gap within the channel was sealed with silicone sealant to prevent sand ingress; the screws connecting the half-probe to the guide bar cut through the sealant relatively easily during a test. The guide bar system provided an effective method to conduct consistent experiments. However one disadvantage was the loss of soil deformation data in an 8 mm wide zone (4 mm on either side of probe axis) ahead of the probe tip where the channel blocked the view of the soil through the Perspex.

Penetration loads were measured using a load cell at the top of the probes as well as strain gauges installed on the probes. **[Reply 3-18] As shown in Fig. 2a, a hemispherical loading cap was attached to the upper part of the load cell. The cap was greased to encourage**

sliding to occur between the actuator loading plate and the upper part of the pile in the event that there was some misalignment between the pile and the actuator which would induce unwanted bending strains within the pile. The probe was hung from the actuator assembly using steel wires to prevent it from penetrating the soil during centrifuge spin-up. Three strain gauges ('SG1', 'SG2' and 'SG3') were embedded inside the body of the half-probe in order to measure tip resistance and shaft friction. Unfortunately, the data obtained from these gauges proved to be unreliable, most likely due to the effect of probe bending and difficulty calibrating the half-probe. For this reason, analysis of cone tip resistance in this paper focuses on data from the full-probe. The full-probe had a similar size and length as the half-probe. As illustrated in Fig. 2b, it was manufactured from aluminium tubing with an outer and inner diameter of $12.7\,mm$ and $9.5\,mm$, respectively. Rather than the single strain gauge in the half-probe tip, a pair of strain gauges ('SG45') were installed on the tip of the full-probe with a Wheatstone half-bridge in order to compensate for bending.

[Fig. 2 about here.]

2.3 Centrifuge tests

Table 1 provides details of the six centrifuge tests presented in this paper. All of the centrifuge tests were carried out on the Nottingham centre for Geomechanics (NCG) $2\,m$ radius geotechnical centrifuge at $50\,g$. Penetration was done at a constant speed of approximately $1\,mm/s$, corresponding to a quasi-static penetration process.

The main focus of this project was the study of penetration within layered soils, which was achieved by varying the relative density of the sand at distinct levels within the soil, as summarised in Table 1. The layered tests included 2-layer soil samples of loose over dense (T04) and dense over loose (T05) sands. These tests intended to reach a 'steady-state' penetration condition within each layer. Two 'sandwich' soil tests (T06 and T07) were also conducted to examine the thin-layer effects during penetration. The results of the two uniform soil tests (T02 and T03) served as a reference for the layered sample tests.

For a particular test, the half-probe test would be done first, then the centrifuge would be spun down and the load actuator moved and fitted with the full-probe before spinning up again to conduct the full-probe test. The test layout is shown in Fig. 1, where the full-probe tests were located to try to reduce the boundary and interaction effects.

[Reply 3-21] Fraction E silica sand, supplied by David Ball Ltd UK, was used for the centrifuge tests due to its appropriate grain size of $d_{50} = 0.14\,mm$, providing a B/d_{50} ratio greater than 20 as suggested by Gui et al. (1998) as well as its high grain

strength, thereby avoiding significant effects of particle breakage. The properties of Fraction E sand as reported by Tan (1990) are listed in Table 2. The mechanical behaviour of Fraction E sand has been investigated by many previous researchers (e.g. Tan, 1990; Bui, 2009). To achieve uniform samples, the multiple-sieving air pluviation method (Miura and Toki, 1982; Zhao, 2008) was employed, with an achievable range of relative density between 50 % and 90 %. A single-holed sand pourer, consisting of a hopper with a nozzle containing multiple sieves, was hung from a hoist for vertical position adjustment and was manoeuvred horizontally by hand in order to fill the centrifuge container. The nozzle of the hopper contains a plate with a single hole, the size of which controls the flow rate of the sand. Calibration tests were carried out using two separate nozzles with hole diameters of $5\,mm$ and $9\,mm$, which provided average flow rates of $0.239\,kg/min$ and $1.048\,kg/min$, respectively. Loose samples ($D_{R,L} \approx 50\,\%$) were prepared using the large nozzle with a pouring height of $0.5\,m$, while dense samples ($D_{R,D} \approx 90\,\%$) were made with the small nozzle at $1\,m$ pouring height. It is worthwhile noting that the loose sample falls within the 'Medium dense' range ($D_R = 35\,\% \sim 65\,\%$) and the dense sample within the 'Very dense' range ($D_R = 85\,\% \sim 100\,\%$), based on BS EN ISO 14688-2 (2004). Layered samples with different sand densities were prepared in the similar manner by changing the nozzle and hopper height during sample preparation.

[Table 1 about here.]

[Table 2 about here.]

3 Results and Discussion

This section presents results obtained from the experiments described in the previous section. Penetration resistance and soil deformation data are presented according to the schematic given in Fig. 3, which also provides an illustration of some other geometric and engineering parameters. The cone tip resistance (q_c) was calculated from the cone tip load, Q_{tip}, (from strain gauge data) divided by the base area (A_b). The total pile load, Q_{total}, was obtained from the load cell at the top of the probe. The depth of penetration is denoted as 'z', soil horizontal and vertical displacements are referred to as Δx and Δy respectively, and 'h' represents the vertical position of a soil element relative to the probe shoulder. All results in this paper are presented in model scale, and compression positive notation is used for the derived strains.

[Fig. 3 about here.]

3.1 Penetration resistance

Fig. 4a provides the development of cone tip resistance q_c with penetration depth for each centrifuge test. As mentioned earlier, the strain gauge data from the half-probe proved to be unreliable, hence the cone tip resistance data presented here is from the full-probe. For penetration in soil with uniform density (T02 and T03), q_c generally increases linearly with z, and the rate at which resistance increases with depth is considerably greater in the uniform dense soil (T02) compared to the uniform loose soil (T03). Bolton et al. (1993), based on the dimensional analysis of CPT results from centrifuge tests and the observed linear relationship between the tip resistance (q_c) and vertical effective stress (σ'_{v0}), proposed the normalised tip resistance, Q, given by

$$Q = \frac{q_c - \sigma'_{v0}}{\sigma'_{v0}} \tag{1}$$

The linear relationship between q_c and z in Fig. 4a indicates that the normalised tip resistance Q is more appropriate for centrifuge penetration tests with a linear stress gradient compared to the non-linear relationships between q_c and σ'_{v0} obtained from calibration chamber tests, where $q_c \propto \sigma'_{v0}{}^{-0.5}$ is typically obtained (Robertson and Wride, 1998; Jamiolkowski et al., 2003). The variation of Q with normalised penetration depth, z/B, is shown in Fig. 4b. Ideally, the tests would have been taken to a greater soil depth and soil interfaces located where the variation of Q with depth remains constant, however this was not possible with the available experimental equipment. This issue does not impact significantly on the conclusions of this analysis since the focus is on the transition of behaviour around the interfaces rather than the absolute values of resistance.

[Fig. 4 about here.]

For layered soil tests, the $q_c - z$ profiles in Fig. 4a show a change in trend (slope) near the soil interfaces. This transition zone is defined as the distance from the cone tip to the soil layer interface when the resistance trend changes. This occurs when the probe is either affected (tip moving towards interface) or is no longer affected (tip moving away from interface) by the soil in the adjacent layer. The size of the transition zone depends on the relative soil properties in the soil layers involved. It was found that the transition zones in dense sands were much larger than that in loose sands. For example, from Fig. 4a, for the test from loose to dense sand (T04), penetration resistance sensed the lower dense sand layer at about $1\,B$ above the soil interface, whereas it took about $4\,B$ below the interface to fully develop the resistance in the dense sand.

It should be noted that the density of the samples in each test is not exactly identical, especially for the loose sands. From calibration tests for sand pouring, the variations of D_R were $90\,\% \pm 5\,\%$ for dense sand and $50\,\% \pm 10\,\%$ for loose sand. Sample inhomogeneity made it difficult to obtain repeatable resistance data. For example, comparing results of T03, T04 and T06, the data in Fig. 4a indicate that the loose sand in T04 was looser than T03, while for T06 the upper loose soil was relatively higher than T03. For this reason, little focus is placed on the absolute values of penetration resistance and emphasis is placed on transitional behaviour around the interfaces.

In order to quantify the transition of q_c between soil layers, the cone tip resistance ratio η, proposed by Xu and Lehane (2008), was defined as $\eta = q_c/q_{c,s}$. For the scenario of penetration from weak soil into strong soil, the value of η varies from $\eta_{min} = q_{c,w}/q_{c,s}$ in the weak soil to $\eta = 1$ in the strong soil. Note that $q_{c,w}$ and $q_{c,s}$ represent the resistances in uniform weak and strong soil, respectively. In view of the good agreement of tip resistance in the upper dense sand layer in tests T02, T05, and T07 illustrated in Fig. 4a, the result of T02 was used as a reference in the strong soil ($q_{c,s}$) to evaluate the resistance ratio for layered soil tests. The resistance ratio curves against the relative distance to the soil interface (z_i/B) are presented in Fig. 5.

[Fig. 5 about here.]

Fig. 5a and b show the results of cone tip resistance ratio for two-layered soils (T04 and T05). Xu and Lehane (2008) performed a series of numerical analyses of spherical cavity expansion to evaluate layered effects on the resistance of piles and penetrometers. According to their parametric study and validation against centrifuge tests, they proposed the following relationship for resistance ratio:

$$\eta = \eta_{min} + (1 - \eta_{min})\, exp[\, -exp\,(A_1 + A_2 \times z_i/B)\,] \tag{2}$$

where $A_1 = -0.22 \ln \eta_{min} + 0.11 \leq 1.5$ and $A_2 = -0.11 \ln \eta_{min} - 0.79 \leq -0.2$. The comparisons of Equation (2) with the current centrifuge results are also provided in Fig. 5a and b, where the value of η_{min} for the Xu and Lehane (2008) line was taken as the resistance ratio obtained using q_c from tests T03 (uniform loose) and T02 (uniform dense) at the soil interface (i.e. $q_{c,min} = q_{c,T03}/q_{c,T02}$, where the subscripts denote the test ID). The small difference in $q_{c,min}$ in Fig. 5a and b is due to the slight variation in interface depth in tests T04 and T05. The experimental data in Fig. 5a should tend towards $\eta = 1$ at high vales of z_i/B; the reason this does not occur is evident from the difference in q_c data for tests T04 and T02 in Fig. 4a, where the T04 data does not tend towards the T02 data at depth as would be expected. As a result, the

agreement between the test T04 data and the Xu and Lehane (2008) prediction in Fig. 5a is not very good in terms of the absolute value of resistance ratio, however the trend and size of the influence zone are both similar. The high values of resistance ratio (greater than 1) for $z_i/B < -5$ in Fig. 5b are a result of the small values of q_c used in the calculation of η nearer the ground surface; the agreement between q_c in the dense soil layer in tests T05 and T02 was actually quite good (see Fig. 4a). So one could assume that the experimental data tended towards $\eta = 1$ at this location, thereby giving a good overall agreement with the Xu and Lehane (2008) prediction.

Also included in Fig. 5 are predictions of resistance ratio using the Mo et al. (2014*a*,*b*) method for interpretation of CPT data in layered soils. This method involves the prediction of the transition of penetration resistance in layered soils using analytical solutions for expanding cavities embedded in two different cohesive-frictional materials. For the analytical prediction, soil model parameters were determined based on the relative density of the soil ($D_R = 50\,\%$ and $D_R = 90\,\%$) using the relationships of Bolton (1986) and Randolph et al. (1994). The in-situ confining pressure for cavity expansion analysis was assumed as the effective vertical stress at the location of the soil interface. The approach of Yasufuku and Hyde (1995) was applied to correlate the cavity pressure to cone resistance. A full description of the analytical methodology is not possible here; readers may refer to (Mo, 2014) for full details.

In Fig. 5a and b, the Mo (2014) prediction is shown to give a larger value of η_{min} than both the experimental and the Xu and Lehane (2008) values, but again the size and trend of the influence zone are predicted well. It should be noted that the value of η_{min} in the Mo (2014) prediction are independent of the experimental measurements of q_c, whereas the Xu and Lehane (2008) value of η_{min} was based on data from tests T03 and T02, as described above. It is therefore not surprising that the Mo (2014) predictions do not agree as well with the experimental data as the ones using Xu and Lehane (2008).

The curves of cone tip resistance ratio for thin-layered soils (T06 and T07) are shown in Fig. 5c and d, where t is the thickness of the sandwiched soil layer and $\eta = q_{c,T06}/q_{c,T02}$ in Fig. 5c and $\eta = q_{c,T07}/q_{c,T02}$ in Fig. 5d. A smaller change in η across the thin layer indicates a greater thin-layer effect, since a value of η that approaches either 1.0 for a thin strong layer (Fig. 5c) or η_{min} for a thin weak layer (Fig. 5d) indicates that the penetration resistance in the thin layer approaches a value typical of a continuous layer of soil. In Fig. 5c, the experimental data of η at low values of $z_i/B < 0$ should tend towards a value of η_{min} which, based on test T04, should have

been about 0.4. From Fig. 4a, it is clear that the values of q_c in test T06 at shallow depths are much greater than the uniform loose test T03, resulting in the very high values of η in Fig. 5c. This may be due to some densification of the soil during model package preparation. In Fig. 5d, the high values of η at shallower depths are a result of the small values of q_c used in the calculation of η, as was the case for the data in Fig. 5b. Considering these points, the experimental data in Fig. 5c and d give a reasonably good idea of the transitional response of penetration resistance in thin-layered soils.

Included in Fig. 5c and d are predictions based on the methodology of Vreugdenhil et al. (1994), which gives an approximate analysis for interpretation of cone penetration results in multi-layer soils by representing a CPT using a circular uniform load. To apply the Vreugdenhil et al. (1994) elastic solution for comparison with the experimental data, a stiffness ratio (G_w/G_s) is required to describe the transition curve, which was assumed to be equal to the resistance ratio (G_w/G_s=$q_{c,w}/q_{c,s}$) obtained using the data from tests T03 ($weak, w$) and T02 ($strong, s$) at a depth midway between the two soil interfaces in tests T06 and T07. The agreement between the Vreugdenhil et al. (1994) predictions and the experimental data are shown to be good, though as for the Xu and Lehane (2008) predictions, the evaluation of η_{min} was based on the experimental data from tests T02 and T03 and was therefore not made independently.

The Mo (2014) analysis approach may also be used to evaluate the trend of penetration resistance in a thin soil layer. Results obtained using this method are included in Fig. 5c and d. In this analysis, the in-situ confining pressure for the cavity expansion analysis was assumed as the effective vertical stress at a depth mid-way between the two soil interfaces. As for the two-layered soils, the method over-predicts the value of η_{min} but provides a good evaluation of the size of the transition zone and a realistic smooth transition of penetration resistance in multi-layered soils.

Also included in Fig 5c are values based on field data for a thin layer of strong soil provided by Youd and Idriss (2001). Empirical equations were used to evaluate the correction factor K_H ($= q_{c,s}/q_{c,max}$, proposed by Robertson and Fear, 1995 to correct the cone resistance from the field measurements) with the thickness of the strong layer (t/B). For t/B = 5.42 in T06, the correction parameter K_H varies from 1.51 to 1.82, and the corresponding maximum value of η is within the range of 0.550 to 0.662. This range of maximum value of η is less than the results of the centrifuge test and the analytical solutions, indicating that this empirical method predicts a greater thin-layer effect.

3.2 Soil displacements

This section presents distributions of displacements associated with the installation of probes under axisymmetric conditions in uniform as well as layered soils. The distributions of soil deformation around the penetrometer provide insights into the mechanisms that are responsible for the probe resistance data presented in the previous section. Using the GeoPIV analysis (White et al., 2003), soil element patches were created by meshing within the field of view in image-space. A patch size of 80 pixels was used which represents a nominal size of $2 \sim 3\,mm$ in object space, according to a particular transformation. The raw GeoPIV data was interpolated to a regular soil mesh in the 'x-y' system (see Fig. 3b) with a grid spacing of $1 \times 1\,mm$ ($x = -6 \sim -120\,mm; y = 0 \sim 200\,mm$), as well as the process of penetration with $1\,mm$ per step. Also, strains were deduced from the displacements based on this re-established mesh. **[Reply 3-29] The results of uniform sand tests (T02 and T03) are presented first in this section to illustrate the effects of penetration depth and the relative density of the soil.** These data also serve as reference for later investigation of layered effects on soil deformation. **It should be recognised that the displacement data was obtained at the soil-Perspex interface and is therefore subject to the effect of boundary friction on displacements. One could expect that some 'slip-stick' behaviour may have occurred, which would cause some spatial variation in the displacement data. Finally, the sample preparation for these tests induced some sample inhomogeneity which may also have caused some variation in observed displacements**.

Fig. 6 presents distributions of displacements at the depth of the probe shoulder ($h = 0$) with offset from the centreline of the probe ($2\,x/B$) when the probe is at different depths within the soil: **[Reply 3]** $z\,/B =$**2.5 to 12.5 (**$z\,/B$ **is the normalised penetration depth). The horizontal and vertical displacements (**$2\,\Delta x/B$**;** $2\,\Delta y/B$**) are also normalised by** B **and represent cumulative values for** $h < 0$**, which means that the displacements are those that occurred from** $z\,/B = 0$ **(initial state) up to the stated penetration depth.** Both lateral and vertical (downwards) displacements are shown to decrease exponentially with horizontal distance from the probe shoulder. This trend is comparable to the results of cavity expansion analysis, as has been noted by several other authors (e.g. Hird et al., 2007; Liu, 2010). The curves also illustrate the decay of the influence of the probe on distant elements. The horizontal size of the influence zone during penetration is $2\,x/B \approx 10$ for dense sand, and slightly smaller for loose sand ($2\,x/B \approx 7$). **For soil elements near the surface, displacements increase with depth, and negative values of** $2\,\Delta y/B$ **in dense sand illustrates heave at the surface.**

[Fig. 6 about here.]

Fig. 7 presents 'instantaneous' total displacement ($=\sqrt{\Delta x^2 + \Delta y^2}$) fields for the uniform dense and loose sand tests. The term 'instantaneous' refers to the displacements that developed over an interval of penetration distance, Δz, (e.g. $\Delta x|_{\Delta z} = \Delta x|_{z+\Delta z/2} - \Delta x|_{z-\Delta z/2}$) and may be used to represent the velocity field at a given penetration stage. This type of plot is useful for illustrating the mechanism of deformation at a given stage of penetration. Fig. 7 relates to a penetration interval distance of $\Delta z = 6\,mm$ when the probe was at a depth of $150\,mm$. The contours are superimposed with displacement vectors to illustrate the direction of movement throughout this interval. The contours are plotted only for values from 0.05 to 1.5, and the vectors were eliminated for displacements less than $0.1\,mm$, which represent soil that hardly deformed during the penetration interval. It may be observed that the influence zone in the instantaneous total displacement field is a bulb around or a bit ahead of the cone tip. Soil elements adjacent to the probe shaft show little deformation, which is mainly caused by the shaft friction. During this interval, the soil in this bulb is displaced horizontally and vertically, and the displacement vectors grow radially, which seems comparable to a spherical cavity expansion. Intuitively, the failure mode is very similar to that proposed by Lee (1990), where zone III (a spherical zone below the probe shoulder) is the spherical cavity expansion zone based on Vesic (1977). This phenomenon also supports the analyses of the correlation between cone penetration and spherical cavity expansion (e.g. Randolph et al., 1994; Yu and Mitchell, 1998; Gui and Jeng, 2009).

The displaced zone in the loose sand is smaller (i.e. the displacement is concentrated closer to the cone tip) than in the dense sand. More downwards movements are observed in the loose sand than the dense sand, whereas dense sand tends to have more lateral displacement than the loose sand. It is also notable that the upper boundary of the influence zone in the dense sand is close to an inclination line at $60\,^\circ$ from vertical, whereas the loose sand has a boundary that inclines at approximately $45\,^\circ$ from vertical.

[Fig. 7 about here.]

The mechanism of soil deformation may also be studied by considering the path or trajectory of a given soil element as it is affected by the probe. Fig. 8 shows trajectories of soil elements at different offsets ($2\,x/B$ = 2, 3, 4, 5, 6) from the probe and at a depth of $y = 120mm$ which were recorded as the probe approached and passed this horizon (up to a penetration distance of $z = 160mm$). Initially, the soil is shown to deform mainly downwards as a result of the probe, however as the probe approaches closer to $y = 120mm$, the soil elements begin to move laterally (the state when the probe shoulder reaches $y = 120mm$ is shown on the figure with a '$\triangle$' denoting $h = 0$). The final state of the soil elements is marked by a '$*$' and the 1:1 line between radial and axial movement ($\Delta x : \Delta y$) is also shown on the figure as a dashed line. The final horizontal displacement of the dense sand is generally a little larger than the vertical displacement; the final position falls to the right of the 1:1 line. For the loose sand, the vertical displacement is observed to be slightly larger than the horizontal displacement at the final state. The magnitude of displacements within the loose sand is also observed to be smaller than in the dense sand. The ratio between the total displacement at the final state of the soil elements in the loose and dense sands decreases from 64 % at $2\,x/B = 2$ to 33 % at $2\,x/B = 6$.

In Fig. 8, the major proportion of displacement is noted to occur during the stage when $h < 0$ (i.e. as the probe approaches the horizon of the soil element), and little contribution is made when $h > 0$ (after the probe shoulder passes). The displacement in the stage when $h > 0$ indicates soil movements away from the probe, which is in contrast with observations by White (2002) who showed that the direction of movement reversed back towards the pile at a magnitude of about 1 % of pile diameter. This led to the conclusion that soil stresses in the region above the probe shoulder were relaxed and that consequently shaft frictional forces were reduced. The data presented here also shows a reversal of displacements near the probe shoulder of approximately 1 % of the pile radius, however it is noted to occur during the stage immediately before the probe shoulder reaches the horizon of the soil element ($-0.5 < h/B < 0$). This difference is probably due to the differing boundary conditions, where the tests here were axisymmetric with a conical tip and the tests reported by White (2002) were plane-strain with a flat-bottomed probe. A comparison of the trends and the magnitude of soil deformation between the two types of models is discussed later in Section 3.3.

[Fig. 8 about here.]

Fig. 9 is an alternative view of the soil element path during penetration which gives an illustration of the soil element distortions that occur during the probe penetration process. The soil elements near the probe are described as $1\,mm \times 1\,mm$ squares. The deformed square elements at different distances from the probe centreline indicate the deformation and distortion patterns within the soil. After the original element is plotted with a '$\circ$', the same element is superimposed every $5\,mm$ of penetration, and the final patch is marked with a '$*$'. The series of soil element patches record the shape of the deformed elements and allow comparison of the element paths between dense and loose sand tests. The deformed shape of the soil elements is noted to be more severe in the dense soil than in the loose soil. The distortion of the soil elements is considered further in the next section which examines soil strains.

[Fig. 9 about here.]

Layered effects on soil displacements

This section presents axisymmetric centrifuge experiment data of the effects of layering on soil displacements. This type of data provides valuable insight into the mechanisms of soil behaviour during penetration problems and has not been provided previously within the literature. This section focuses on the results of soil deformation for tests with layered soils (T04 to T07).

The profiles of normalised cumulative vertical displacements ($2\,\Delta y/B$) for soil at an offset of $2\,x/B = 2$ in the uniform and layered sand tests are provided in Fig. 10. From the results of $2\,\Delta y/B$ in loose over dense sand (T04 in Fig. 10a), the peak above the interface occurs at around $2\,B$, where the penetration resistance starts to be affected. The influence zone beneath the interface is not as obvious due to the smooth nature of the curves, however the data tends to level off at about $5B$ from the interface, which is close to the value of $z_s = 4B$ from the penetration resistance data in Fig. 5a. For the test with dense over loose sand (T05 in Fig. 10b), the peak occurs at the interface, and it is not possible to define an influence zone in the strong overlying soil due to the cumulative soil deformation. Comparing the result with the trend of dense sand in T02, the soil starts to be affected at about $5\,B$ above the loose sand layer. The influence zone in loose sand appears to be about $4\,B$, based on the point at which the Δy profile levels out. The thin-layer effects on soil displacements for T06 and T07 are also presented in Fig. 10 and compared against the corresponding 2-layer test as well as the uniform soil tests. For test T06, the vertical displacement in the sandwiched dense layer increases steadily and reaches a maximum value just above the dense-loose soil interface. For test T07, the vertical displacement decreases steadily within the sandwiched loose sand layer and reaches a minima just above the loose-dense soil interface. Comparing the influence zones in soil deformation with that in penetration resistance, it is found that the sizes are different but correlated. Due to the limited tests in this paper, further study on the penetration mechanisms is required to investigate the relationship between the layered effects on both penetration resistance and soil deformation.

[Fig. 10 about here.]

3.3 Soil strains

This section presents soil strains which were derived from the incremental displacement data introduced in the previous section. The calculation of strains was done by importing the measured displacement fields into a corresponding mesh within the finite difference software FLAC (Itasca, 2005) for each step of penetration, as suggested by Marshall (2009). Based on the axisymmetric condition of the experiments with Cauchy's infinitesimal strain tensor and a small deformation assumption, the strains were calculated using:

$$\begin{aligned}
&\epsilon_{xx} = -\frac{\partial\,\Delta x}{\partial\,|x|} && \epsilon_{yy} = -\frac{\partial\,\Delta y}{\partial\,y} && \epsilon_{xy} = -\frac{1}{2}\left(\frac{\partial\,\Delta x}{\partial\,y} + \frac{\partial\,\Delta y}{\partial\,|x|}\right) \\
&\epsilon_{\theta\theta} = -\frac{\Delta x}{|x|} && \epsilon_{x\theta} = \epsilon_{y\theta} = 0 && \epsilon_{volume} = \epsilon_{xx} + \epsilon_{yy} + \epsilon_{\theta\theta}
\end{aligned} \tag{3}$$

The Mohr circle of strains in the 'x-y' plane is illustrated in Fig. 11a. Some smoothing was applied to the strain data presented in this section in order to deal with the amplification of scatter obtained when calculating strains from the GeoPIV displacement data.

Fig. 11c-d shows the instantaneous strain fields with magnitude and direction of principal strain rate at a penetration depth of $z = 150\,mm$ **[Reply 3-39] and resulting from a probe displacement increment of** $6\,mm$ **(i.e.** $\epsilon\,|_{\Delta z} = \epsilon\,|_{z+\Delta z/2} - \epsilon\,|_{z-\Delta z/2}$**)**. The principal strain rates of $\dot{\epsilon}_1$ and $\dot{\epsilon}_2$ from the 'x-y' plane (refer to Fig. 11b) are shown, where $\dot{\epsilon}_1$ is compression and $\dot{\epsilon}_2$ is tension. The magnitude of strain rate is illustrated by the size of the crossing lines (a standard length for $10\,\%$ strain rate is given in the plots). The main principal strain rate is directed from the cone tip, and decays significantly with relative distance. Despite the fact that sand is known to behave in a non-coaxial manner, the large strain around the probe cone leads to a reduced effect of non-coaxiality (Roscoe, 1970). Hence the directions of the principal strain rate provides some clues for estimation of directions and distributions of the principal stress rate. The directions of the principal strain rate between dense and loose sand are observed to be similar, with slightly smaller inclination from vertical for the loose sample.

[Fig. 11 about here.]

Strain paths shown in Fig. 12 reveal the evolution of strains (ϵ_{xx}, ϵ_{yy}, ϵ_{xy}, ϵ_{volume}, $\epsilon_{\theta\theta}$, ϵ_1, ϵ_2) during probe installation. The strain histories are plotted against the relative position from the probe shoulder (h/B) for soil elements in the near field ($2\,x/B = 2$) at a depth of $120\,mm$ for both dense and loose sand tests. The majority of the strain is shown to develop before the probe shoulder passes, and the strain remains nearly constant when $h > 0$.

[Fig. 12 about here.]

In Fig. 12, the strain reversal of ϵ_{xx} and ϵ_{yy} occurs before the probe shoulder passes. With penetration, ϵ_{xx} gradually drops to a minimum at $h/B \approx -2$, which is slightly earlier than when ϵ_{yy} reaches its maximum, followed by the phase of strain reversals. The strains change direction and reach an opposite peak at $h/B \approx -0.5$. The location where these two curves intersect suggests that the relatively small compressive strains (ϵ_{xx} and ϵ_{yy}) occur at $h/B \approx -1$, where ϵ_{xy} grows sharply to its maximum value. The value of shear strain in dense sand is larger than that in loose sand, which is also in accordance with the distorted soil element patches shown in Fig. 9. There is no obvious difference in the strain reversal for both dense and loose sand. The sensing distances of ϵ_{xx} and ϵ_{yy} are shown to be about $8\,B$ in the dense sand and $5\,B$ in the loose sand. These sensing distances may be compared to the influence zones in layered soils determined earlier from the penetration resistance data. It was noted that the influence zone in dense soil was larger than in loose soil, which agrees with the sensing distances determined from Fig. 4.

The phase from $h/B = -0.5$ to 0 exhibits a small proportion of strain reduction, which is most notable in the ϵ_{xy} data for the dense sand. The two principal strains (ϵ_1 and ϵ_2) represent the size of the Mohr circle in the 'X Y' plane. Extensive $\epsilon_{\theta\theta}$ is the minimum principal strain and continuously grows until the probe almost reaches the soil element horizon. Consequently, the negative volumetric strain indicates the dilatant behaviour of the soil near the probe, whereas the final state of loose sand appears to have nearly no dilation; this can be attributed to the relatively high compressive ϵ_{xx} values in Fig. 12b.

The phenomenon of strain reversal discussed above was also reported by Baligh (1985) and White and Bolton (2004). However, the former was an analytical solution that is only suitable to undrained clay and the latter was from calibration chamber tests in a plane-strain model. The strain data from the axisymmetric model presented here, and in particular the strain reversal behaviour illustrated in Fig. 12, are most applicable to conventional penetration problems in sand.

The variation of ϵ_{volume} with offset from the probe centreline is shown in Fig. 13 for $y = 150\,mm$. The eventual state of ϵ_{volume} also indicates the distribution of density after penetration. For dense sand, the soil elements at $2\,x/B = 2 \sim 4$ show a peak dilation when the probe is just above the soil element horizon ($h/B = -1 \sim -2$), followed by a quick transition to a final dilative state. For the soil elements further away, there is a general increase in volumetric strain towards the ultimate contractive state value. For the loose soil, there is no systematic trend in final volumetric strain with offset. All the soil elements illustrate a final contractive state and the magnitude of contractive volumetric strain is generally higher compared to the dense soil.

[Fig. 13 about here.]

The effect of the axisymmetric condition of the tests conducted as part of this project are illustrated in Fig. 14 by comparing soil strains against results from plane-strain tests reported by White (2002). The tests conducted by White (2002) used a $32.2\,mm$ plane-strain probe and a calibration chamber with Fraction B silica sand, which is a larger grading of the same silica sand used in these tests (D_{50} of Fraction B is $0.84\,mm$ whereas it is $0.14\,mm$ for Fraction E). The ratio of probe diameter to average grain size (B/d_{50}) for the tests reported by White (2002) was 86, whereas it was 38 for the centrifuge tests. All of the soil elements were selected at a similar distance from the probe centreline ($2\,x/B = 2$ and 1.99). The data for the axisymmetric test was taken at a depth of $120\,mm$ with an initial vertical stress of $90\,kPa$, while the data from the plane-strain test was under an isotropic stress condition of approximately $50\,kPa$.

Fig. 14 shows the horizontal and vertical strain at $2\,x/B = 2$ for the two test configurations. The data shows that, compared to the axisymmetric test, the plane-strain test illustrated higher vertical compressive strains before the probe passed the soil element and that the peak vertical strain occurred earlier. Horizontal strains were considerably larger in the plane-strain test during the stage when the probe approached the soil element, and ultimately stayed in a tensile state whereas they went to a compressive state in the axisymmetric test. The higher horizontal strains in the plane-strain tests can be attributed to the fact that the degree of freedom of the soil in the out-of-plane direction is restricted in these tests, therefore the in-plane horizontal and vertical strains respond to a greater degree due to the probe penetration. As a direct consequence of this, the sensing distance for the plane-strain test is greater than the axisymmetric test, as indicated in Fig. 14 where the strains begin to change at about $-10\,B$ for the plane-strain test and $-8\,B$ for the axisymmetric test.

[Fig. 14 about here.]

Layered effects on soil strains

The results of soil strains for the tests with layered soils are presented in this section. As shown in Fig. 13, the volumetric strains are relatively dilative in dense sand and contractive in loose sand. Fig. 15 shows the results of volumetric strain paths for soil elements at $2\,x/B = 2$ with variation of distance to the soil interface for the 2-layered soil tests. The strain paths far away from the interface have similar trends to those from the uniform tests. For the loose over dense test (Fig. 15a), a transition of the trends from characteristically loose to dense occurs. For the dense over loose test (Fig. 15b), there is also a transition of the trends, however the data obtained when the probe was at the interface ($y = y_{int}$) shows somewhat unexpectedly high values of contraction which are not fully understood and may be a result of errors associated in the calculation of strains. The transition zones for both tests are within a distance of about $2\,B$ from the interface.

[Fig. 15 about here.]

Fig. 16 provides the cumulative volumetric strain profiles for $2\,x/B = 2$ after $160\,mm$ of penetration. The ultimate value of ϵ_{volume} after the probe has passed a given location is about $0\,\%$ in loose sand and approximately $-6\,\%$ in dense sand. **[Reply1-12] The variation of the data within the uniform soil tests is attributed to the issues identified earlier, namely the effects of boundary friction, the scatter in the PIV data and its effect on calculated strains, and the soil inhomogeneity caused by sample preparation.** For the layered tests, there is a transition of ϵ_{volume} from these values within a rather small zone which is about $2\,B$ in size.

[Fig. 16 about here.]

4 Conclusions

A series of full- and half-probe cone penetration tests were performed in various configurations of silica sand in a 180° axisymmetric model container. The centrifuge penetration tests, together with soil deformation measurement, provided an effective approach for investigation of penetration mechanisms around the probe. Uniform dense and loose sand tests showed a linear increase of total load and tip resistance with depth. A transition of tip resistance was observed within a zone of influence around the layered soil interfaces. The tip resistance ratio η, proposed by Xu and Lehane (2008), was used to illustrate the transition of q_c from one soil layer to another. The influence zone in stronger soil was larger than that in weaker soil and was also dependant on the direction of probe travel. The characteristics of the influence zone were shown to be important for thin-layer soil profiles where a 'steady-state' condition may not be reached within the thin layer, depending on the relative properties of the soil layers.

The use of spherical cavity expansion methods for analysis of penetration problems was supported by the observation of the instantaneous soil displacement around the cone tip. From the trajectories of soil elements, it was noted that the major proportion of the displacement occurred before the probe passed, and little contribution was made during $h > 0$. In addition, the directions of the principal strain rate provided some clues for estimation of directions and distributions of the principal stress rate. Strain reversal during penetration in the axisymmetric model was also quantified to indicate the severe distortion with rotation and dilation. The results of deformation were also compared with data from White (2002) to examine the effect of particle size and to illustrate the differences between plane-strain and axisymmetric tests.

The mechanism of deformation of layered soils around the probe was described and highlighted using displacement and strain profiles. The variation of soil displacement with different profiles of soil density illustrated the layering effect on soil displacement mechanisms. The layered effects on soil strains were also investigated through the transitions of the strain paths and distributions of cumulative volumetric strains.

List of notation

Δx, Δy horizontal and vertical displacements

ϵ strain

η pile end bearing resistance ratio, proposed by Xu and Lehane (2008)

$\sigma'_{v\,0}$ initial vertical stress

A_b base area of probe

B diameter of penetrometer

D diameter of centrifuge container

D_R relative density of soil

d_{50} grain diameter for which 50 % of the sample (by weight) is smaller

e void ratio of sand sample

G_s specific gravity

h vertical position of soil element relative to probe shoulder

K_H correction factor for thin-layer effects

Q normalised cone tip resistance

q_c cone tip resistance

Q_{total}, Q_{tip} total penetration load and tip load

t thickness of sandwiched soil layer

x, y horizontal and vertical locations of soil elements

z depth of penetration

z_i distance to soil interface

FOV field of view

GeoPIV geotechnical Particle Image Velocimetry

NCG Nottingham Centre for Geomechanics

References

Ahmadi, M. M. and Robertson, P. K. (2005), 'Thin-layer effects on the CPT q(c) measurement', *Canadian Geotechnical Journal* **42**(5), 1302–1317.

Baligh, M. (1985), 'Strain path method', *ASCE Journal of Geotechnical Engineering* **111**(9), 1108–1136.

Bolton, M. D. (1986), 'The strength and dilatancy of sands', *Géotechnique* **36**(1), 65–78.

Bolton, M. D., Gui, M. W. and Phillips, R. (1993), Review of miniature soil probes for model tests, *in* 'Proc. 11th South East Asia Geotechnical Conf.', pp. 85–91.

BS EN ISO 14688-2 (2004), 'Geotechnical investigation and testing. identification and classification of soil. principles for a classification', *London: British Standards Institution* .

Bui, M. T. (2009), Influence of some particle characteristics on the small strain response of granular materials, PhD thesis, University of Southampton.

Gui, M., Bolton, M. D., Garnier, J., Corte, J. F., Bagge, G., Laue, J. and Renzi, R. (1998), Guidelines for cone penetration tests in sand, *in* 'International Conference on Centrifuge Modelling (Centrifuge '98)', Vol. 1, Balkema, pp. 155–160.

Gui, M. W. and Jeng, D. S. (2009), 'Application of cavity expansion theory in predicting centrifuge cone penetration resistance', *The Open Civil Engineering Journal* **3**, 1–6.

Hird, C. C., Emmett, K. B. and Davis, G. (2007), Piling in layered ground: Risk to groundwater and archaeology, Technical Report SC020074/SR, The Environment Agency.

IRTP (1994), International reference test procedure (IRTP) for the Cone Penetration Test (CPT) and the Cone Penetration Test with pore pressure (CPTU), *in* 'Proceedings of the XIIth ECSMGE', Balkema, pp. 2195–2222.

Itasca (2005), 'FLAC-3D user's manual'.

Jamiolkowski, M., Lo Presti, D. C. F. and Manassero, M. (2003), 'Evaluation of relative density and shear strength of sands from CPT and DMT', *Soil Behavior and Soft Ground Construction* **7**(119), 201–238.

Jardine, R. J. and Chow, F. C. (1996), New design methos for offshore piles, Technical Report MTD96/103, Marin Tech. Directorate.

Lee, S. (1990), Centrifuge modelling of cone penetration testing in cohesionless soils, PhD thesis, University of Cambridge.

Lehane, B. M., Schneider, J. A. and Xu, X. (2005), The UWA-05 method for prediction of axial capacity of driven piles in sand, *in* 'International Symposium on Frontiers in Offshore Geotechnics', pp. 683–689.

Liu, W. (2010), Axismmetric centrifuge modelling of deep penetration in sand, PhD thesis, University of Nottingham.

Marshall, A. M. (2009), Tunnelling in sand and its effect on pipelines and piles, PhD thesis, Cambridge University.

Marshall, A. M. and Mair, R. J. (2011), 'Tunneling beneath driven or jacked end-bearing piles in sand', *Canadian Geotechnical Journal* **48**(12), 1757–1771.

Miura, S. and Toki, S. (1982), 'A sample preparation method and its effect on static and cyclic deformation-strength properties of sand', *Soils and Foundations* **22**, 61–77.

Mo, P. Q. (2014), Centrifuge modelling and analytical solutions for the cone penetration test in layered soil, PhD thesis, University of Nottingham.

Mo, P. Q., Marshall, A. M. and Yu, H. S. (2014*a*), 'Cavity expansion analysis for interpretation of cpt data in layered soils', *3rd Internationa Symposium on Cone Penetration Testing, Las Vegas, Nevada, USA* pp. 331–338.

Mo, P. Q., Marshall, A. M. and Yu, H. S. (2014*b*), 'Elastic-plastic solutions for expanding cavities embedded in two different cohesive-frictional materials', *International Journal for Numerical and Analytical Methods in Geomechanics* **38**(9), 961–977.

Moss, R. E. S., Seed, R. B., Kayen, R. E., Stewart, J. P., Kiureghian, A. D. and Cetin, K. O. (2006), 'CPT-based probabilistic and deterministic assessment of in situ seismic soil liquefaction potential', *Journal of Geotechnical and Geoenvironmental Engineering* **132**(8), 1032–1051.

Randolph, M. F., Dolwin, J. and Beck, R. (1994), 'Design of driven piles in sand', *Géotechnique* **44**(3), 427–448.

Robertson, P. K. (1982), In-situ tesing of soil with emphasis on its application to liquefaction assessment, PhD thesis, The University of British Columbia.

Robertson, P. K. and Fear, C. E. (1995), Liquefaction of sands and its evaluation, *in* 'Proceedings of the 1st International Conference on Earthquake Geotechnical Engineering', Vol. 3, pp. 1253–1289.

Robertson, P. K. and Wride, C. E. (1998), 'Evaluating cyclic liquefaction potential using the cone penetration test', *Canadian Geotechnical Journal* **35**(3), 442–459.

Roscoe, K. H. (1970), 'The influence of strains in soil mechanics', *Géotechnique* **20**(2), 129–170.

Silva, M. F. and Bolton, M. D. (2004), 'Centrifuge penetration tests in saturated layered sands', *Geotechnical and Geophysical Site Characterization Vols 1 and 2* pp. 377–384.

Tan, F. S. C. (1990), Centrifuge and theoretical modelling of conical footings on sand, PhD thesis, University of Cambridge.

Treadwell, D. D. (1976), The influence of gravity, prestress, compressibility, and layering on soil resistance to static penetration, PhD thesis, University of California at Berkeley.

Tseng, D. J. (1989), Prediction of cone penetration resistance and its application to liquefaction assessment, PhD thesis, University of California, Berkeley, Calif.

van den Berg, P., de Borst, R. and Huetink, H. (1996), 'An eulerean finite element model for penetration in layered soil', *International Journal for Numerical and Analytical Methods in Geomechanics* **20**, 865–886.

Vesic, A. S. (1977), Design of pile foundations, Technical report, Transport Research Board.

Vreugdenhil, R., Davis, R. and Berrill, J. (1994), 'Interpretation of cone penetration results in multilayered soils', *International Journal for Numerical and Analytical Methods in Geomechanics* **18**(9), 585–599.

Walker, J. and Yu, H. S. (2010), 'Analysis of the cone penetration test in layered clay', *Géotechnique* **60**(12), 939–948.

White, D. J. (2002), An investigation into the behaviour of pressed-in piles, PhD thesis, Cambridge University.

White, D. J. and Bolton, M. D. (2004), 'Displacement and strain paths during plane-strain model pile installation in sand', *Géotechnique* **54**(6), 375–397.

White, D. J. and Bolton, M. D. (2005), 'Comparing CPT and pile base resistance in sand', *Proceedings of the Institution of Civil Engineers-Geotechnical Engineering* **158**(1), 3–14.

White, D. J., Take, W. A. and Bolton, M. D. (2003), 'Soil deformation measurement using particle image velocimetry (PIV) and photogrammetry', *Géotechnique* **53**(7).

Xu, X. T. (2007), Investigation of the end bearing performance of displacement piles in sand, PhD thesis, The University of Western Australia.

Xu, X. T. and Lehane, B. M. (2008), 'Pile and penetrometer end bearing resistance in two-layered soil profiles', *Géotechnique* **58**(3), 187–197.

Yasufuku, N. and Hyde, A. F. L. (1995), 'Pile end-bearing capacity in crushable sands', *Géotechnique* **45**(4), 663–676.

Youd, T. L. and Idriss, I. M. (2001), 'Liquefaction resistance of soils: Summary report from the 1996 NCEER and 1998 NCEER/NSF workshops on evaluation of liquefaction resistance of soils', *Journal of Geotechnical and Geoenvironmental Engineering* **127**(4), 297–313.

Yu, H. S. and Mitchell, J. K. (1998), 'Analysis of cone resistance: Review of methods', *Journal of Geotechnical and Geoenvironmental Engineering* **124**(2), 140–149.

Zhao, Y. (2008), In situ soil testing for foundation performance prediction, PhD thesis, University of Cambridge.

List of Figures

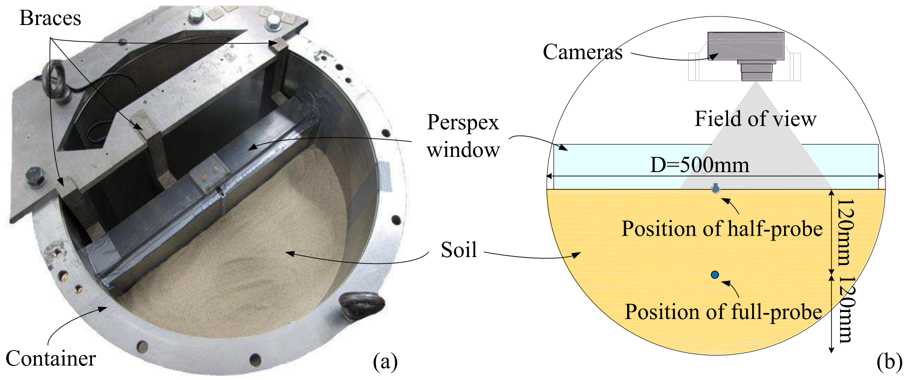

Fig. 1: The centrifuge container with Perspex window

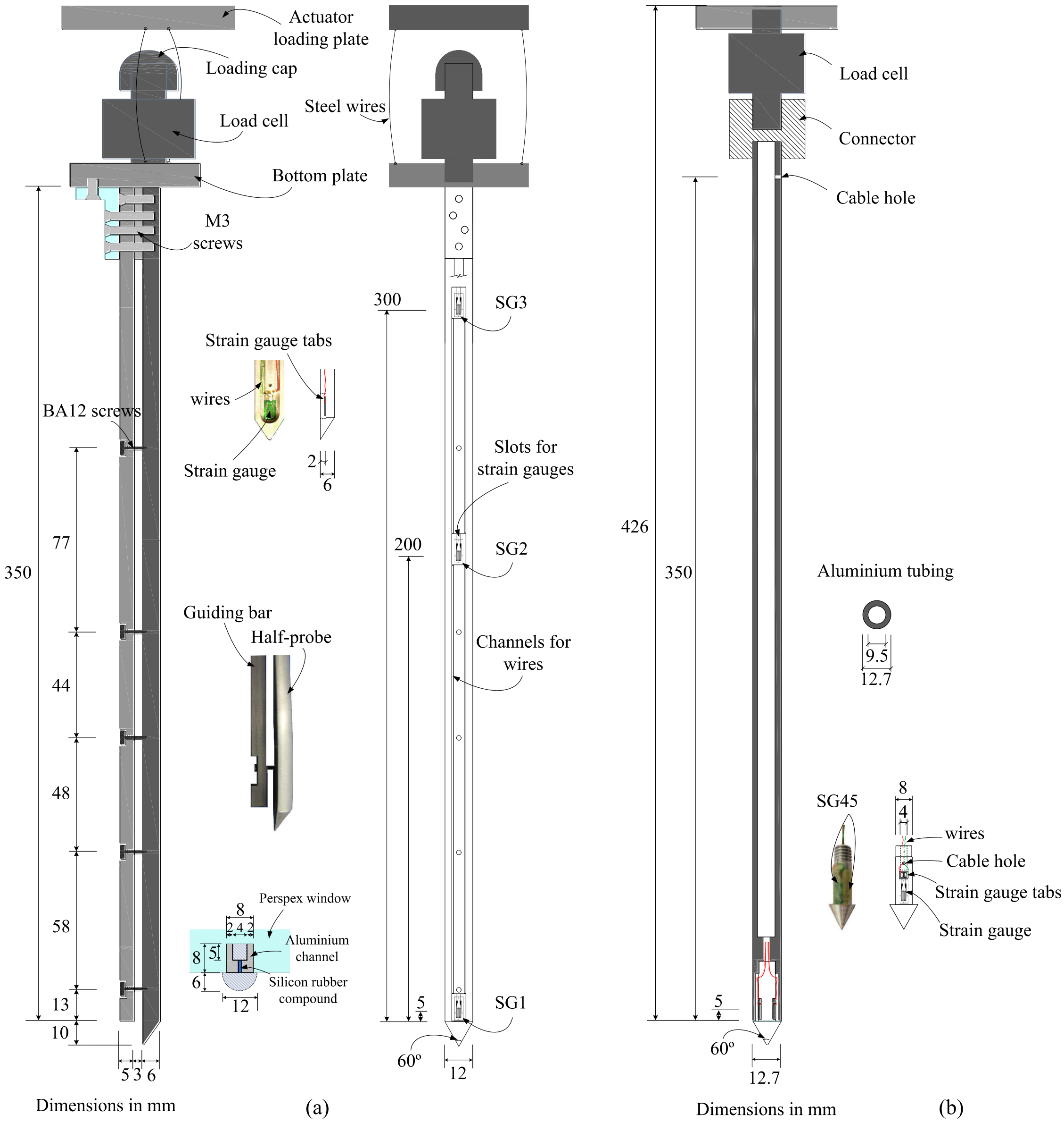

Fig. 2: Schematic of (a) the half-probe assembly; and (b) the full-probe assembly

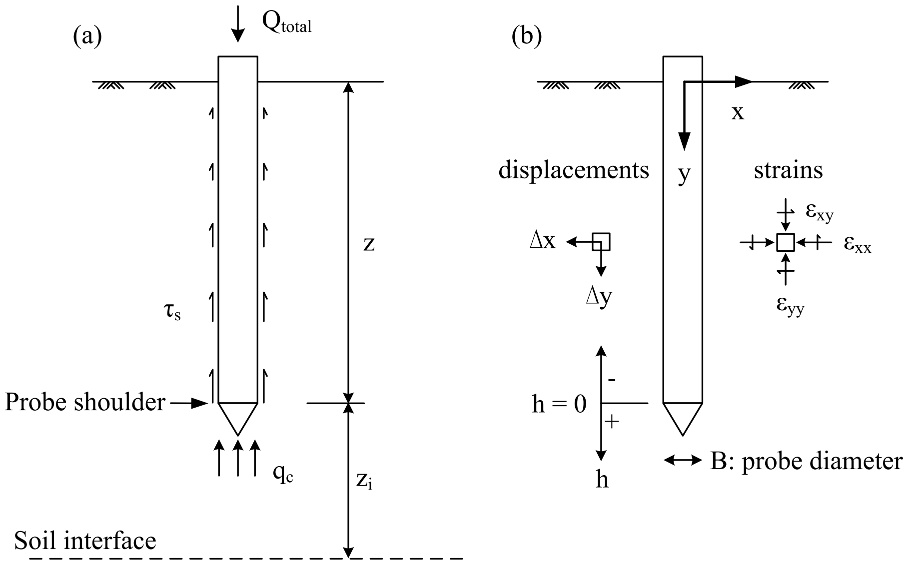

Fig. 3: Schematics of (a) penetration resistance and (b) soil deformation

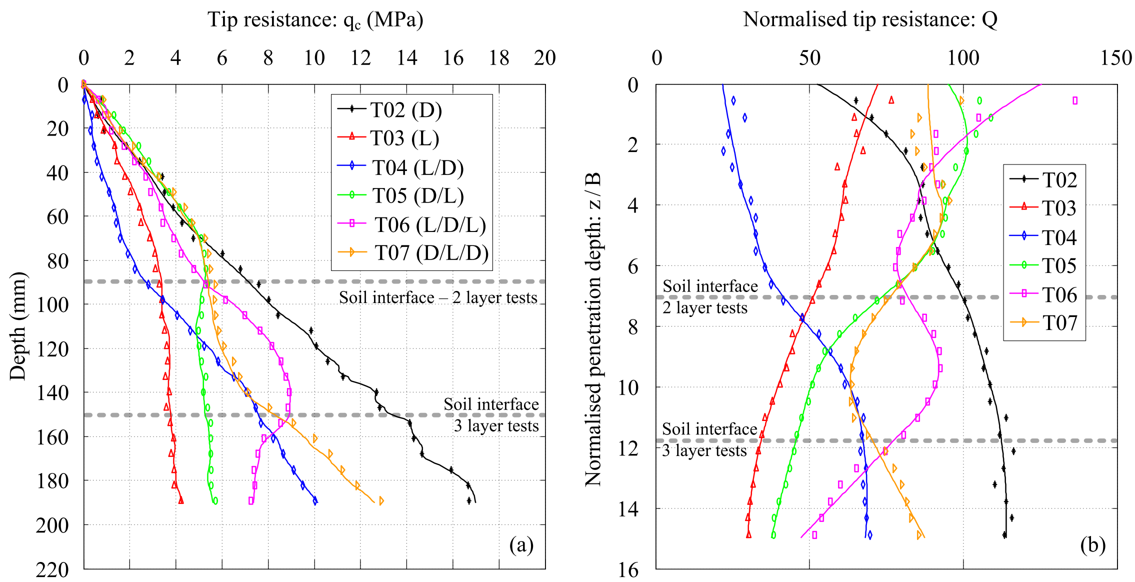

Fig. 4: Results of penetration resistance: (a) cone tip resistance against depth; (b) normalised tip resistance against normalised depth

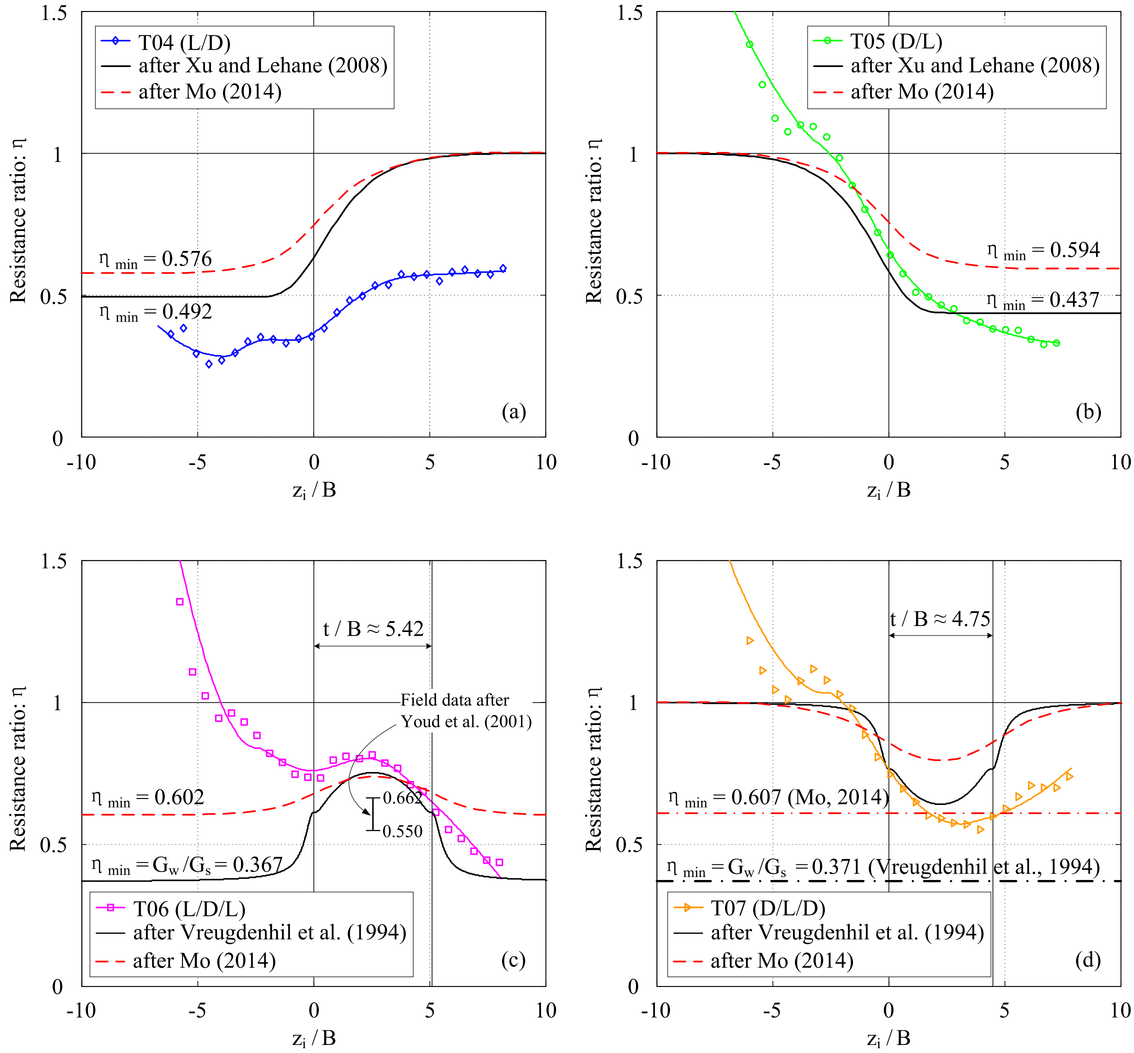

Fig. 5: Resistance ratio against relative distance to soil interface: (a) T04; (b) T05; (c) T06; (d) T07

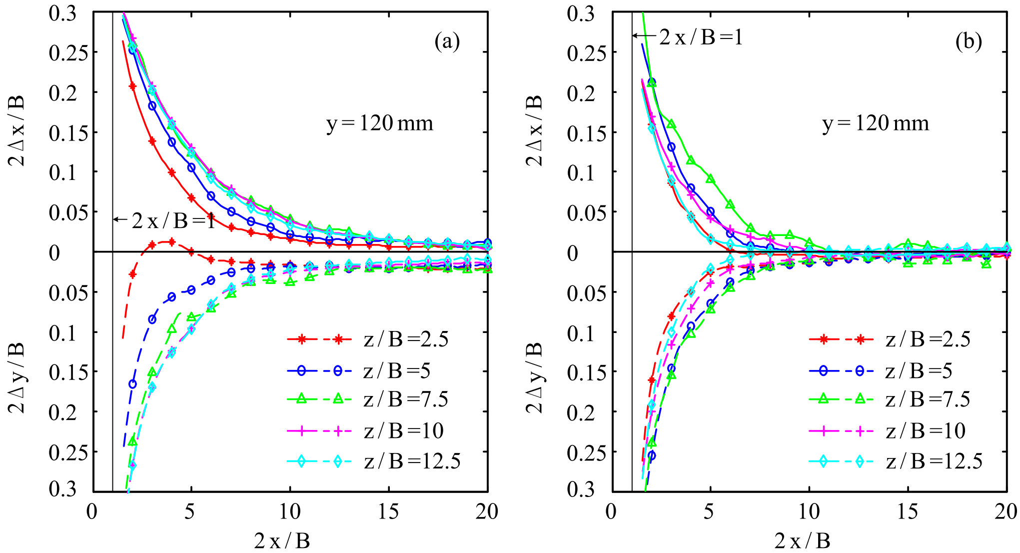

Fig. 6: Displacement distributions ($h = 0$) with variation of penetration depth: (a) T02: Dense sand ($D_R = 90\,\%$); (b) T03: Loose sand ($D_R = 50\,\%$)

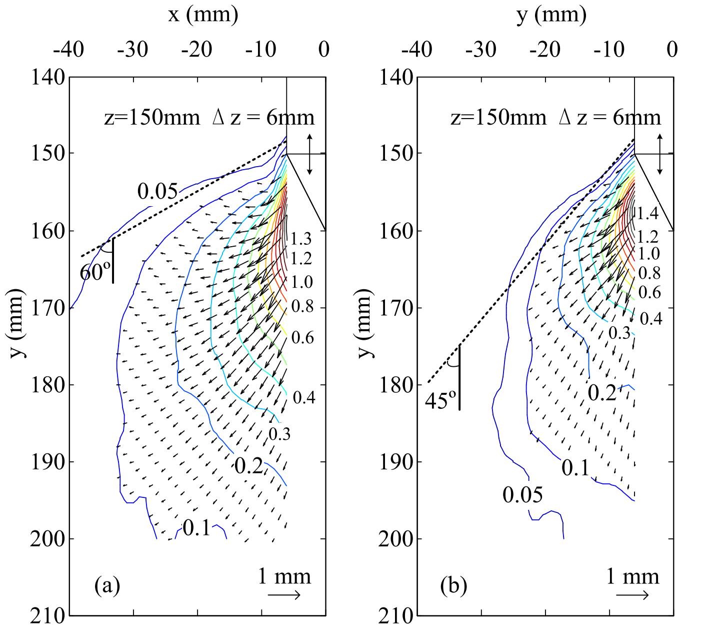

Fig. 7: Instantaneous displacement contours for: (a) T02: Dense sand ($D_R = 90\,\%$); (b) T03: Loose sand ($D_R = 50\,\%$)

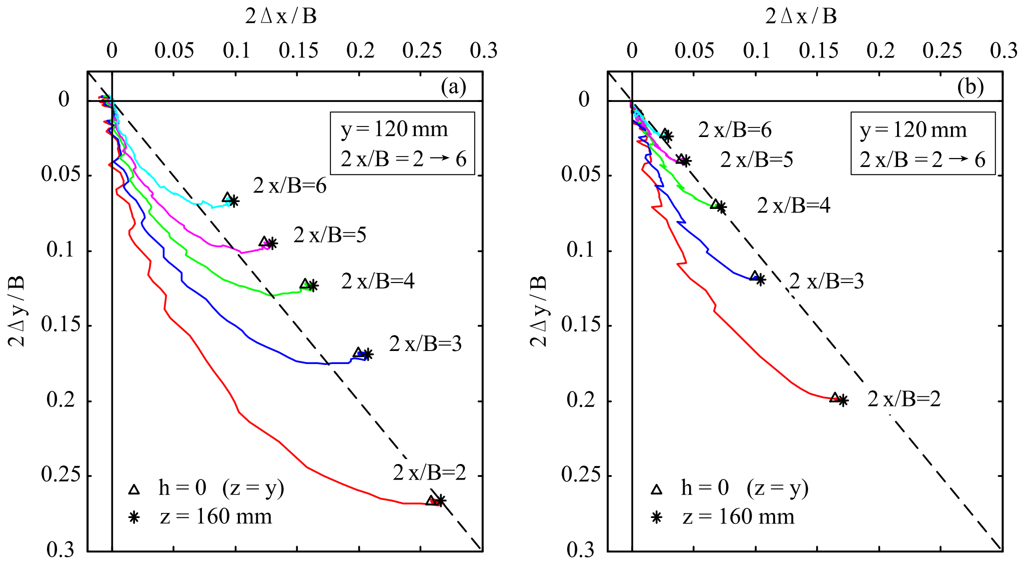

Fig. 8: Trajectories of soil elements at depth $y = 120\,mm$ with variation of $2\,x/B$: (a) T02: Dense sand ($D_R = 90\,\%$); (b) T03: Loose sand ($D_R = 50\,\%$)

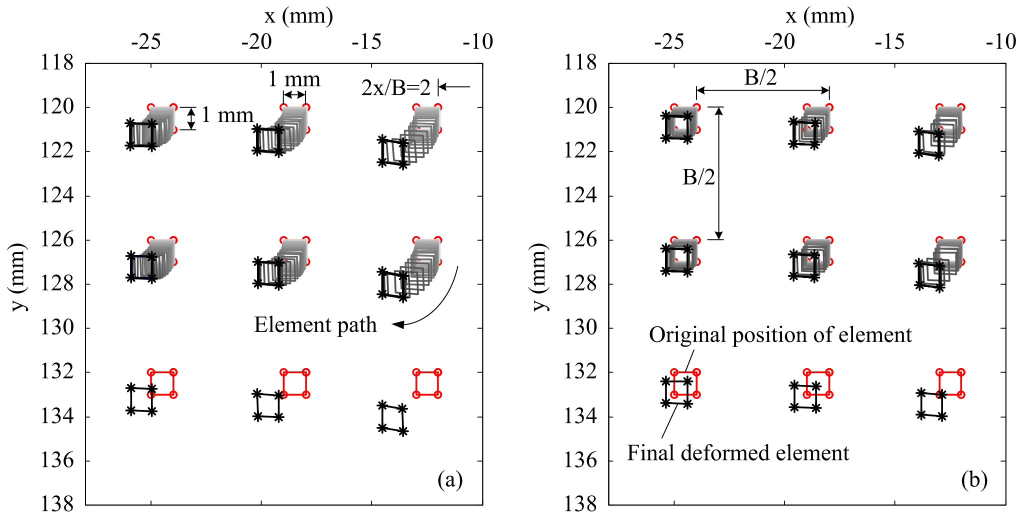

Fig. 9: Soil element path during 150 mm of penetration: (a) T02: Dense sand ($D_R = 90\,\%$); (b) T03: Loose sand ($D_R = 50\,\%$)

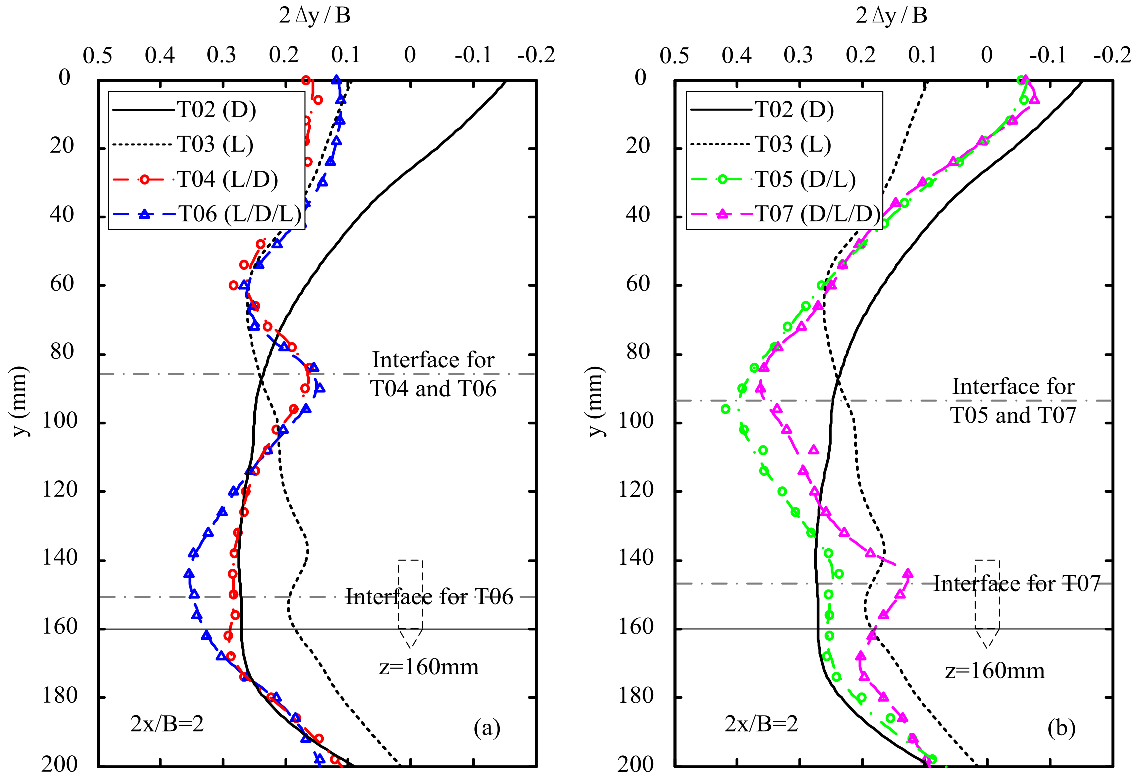

Fig. 10: Cumulative vertical displacement profiles for $2\,x/B = 2$ after 160 mm of penetration: (a) T04 and T06; (b) T05 and T07

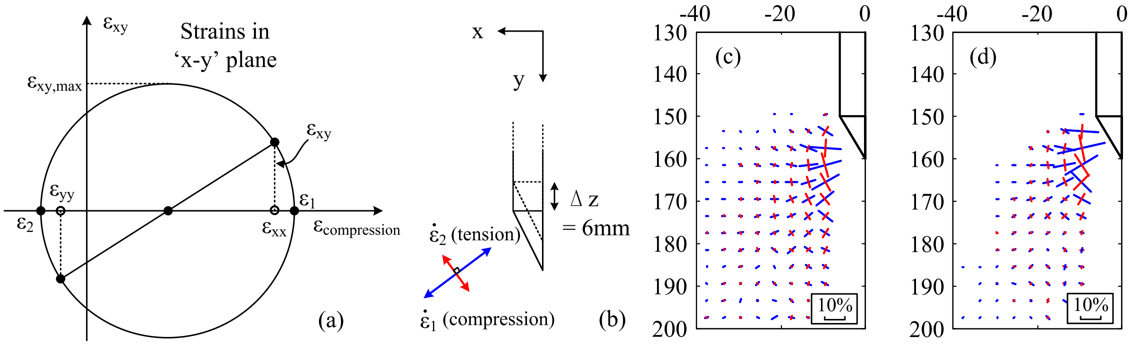

Fig. 11: Mohr circle of strains (a) and Principal strain rates (b) at penetration depth of 150 mm for: (c) T02: Dense sand ($D_R = 90\,\%$); (d) T03: Loose sand ($D_R = 50\,\%$)

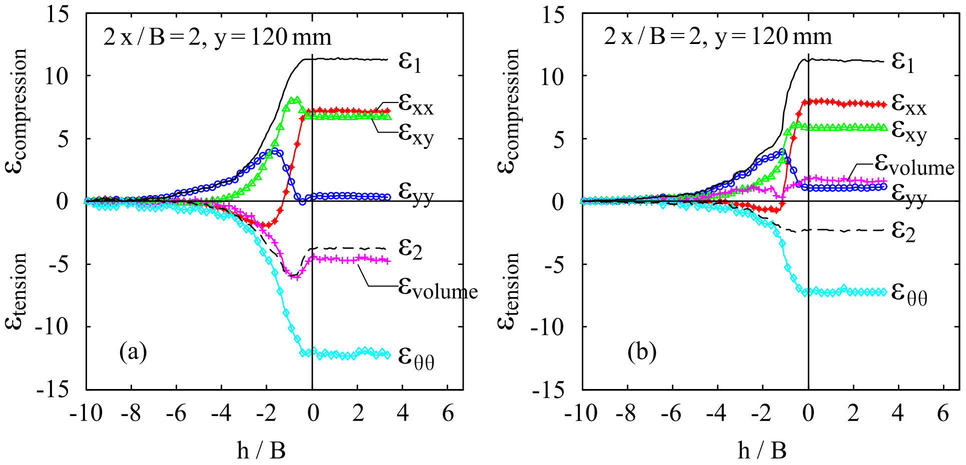

Fig. 12: Strain paths of soil element at $2\,x/B = 2$ and $y = 120\,mm$ against h/B: (a) T02: Dense sand ($D_R = 90\,\%$); (b) T03: Loose sand ($D_R = 50\,\%$)

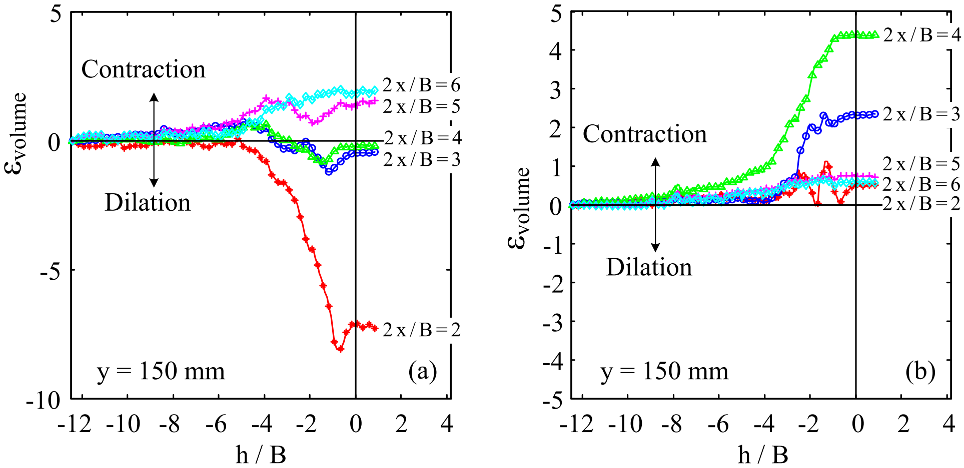

Fig. 13: Volumetric strain paths of soil elements at $2\,x/B = 2 \rightarrow 6$ and $y = 150\,mm$ against h/B: (a) T02: Dense sand ($D_R = 90\,\%$); (b) T03: Loose sand ($D_R = 50\,\%$)

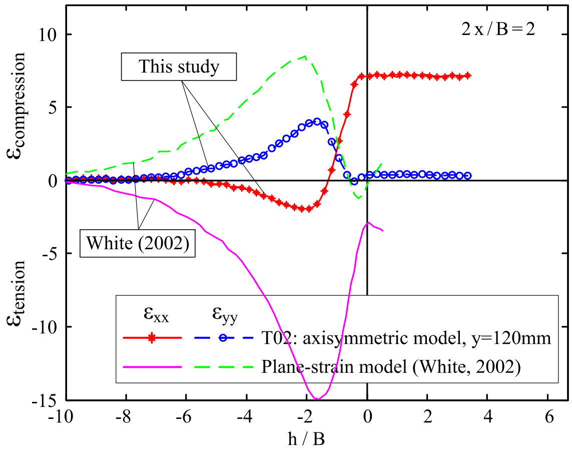

Fig. 14: Comparison between soil strains from axisymmetric and plane-strain penetration tests

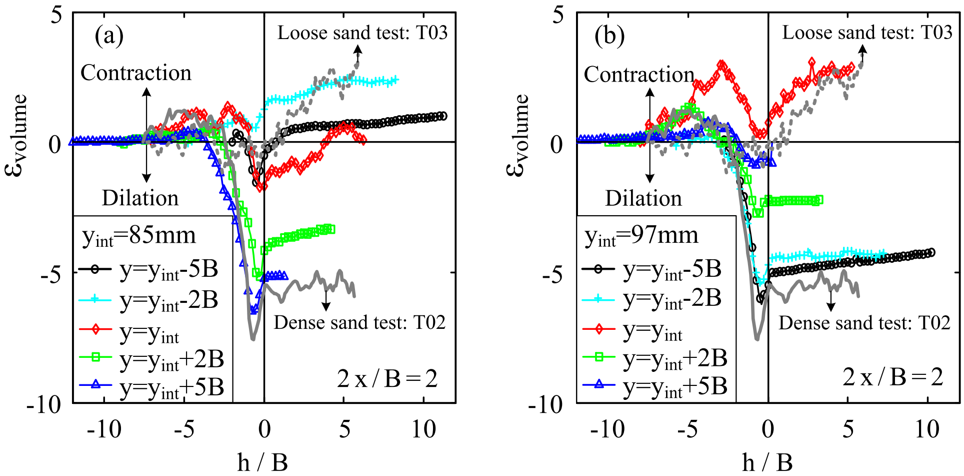

Fig. 15: Volumetric strain paths of soil elements at $2\,x/B = 2$ with variation of depth: (a) T04 (L/D); (b) T05 (D/L)

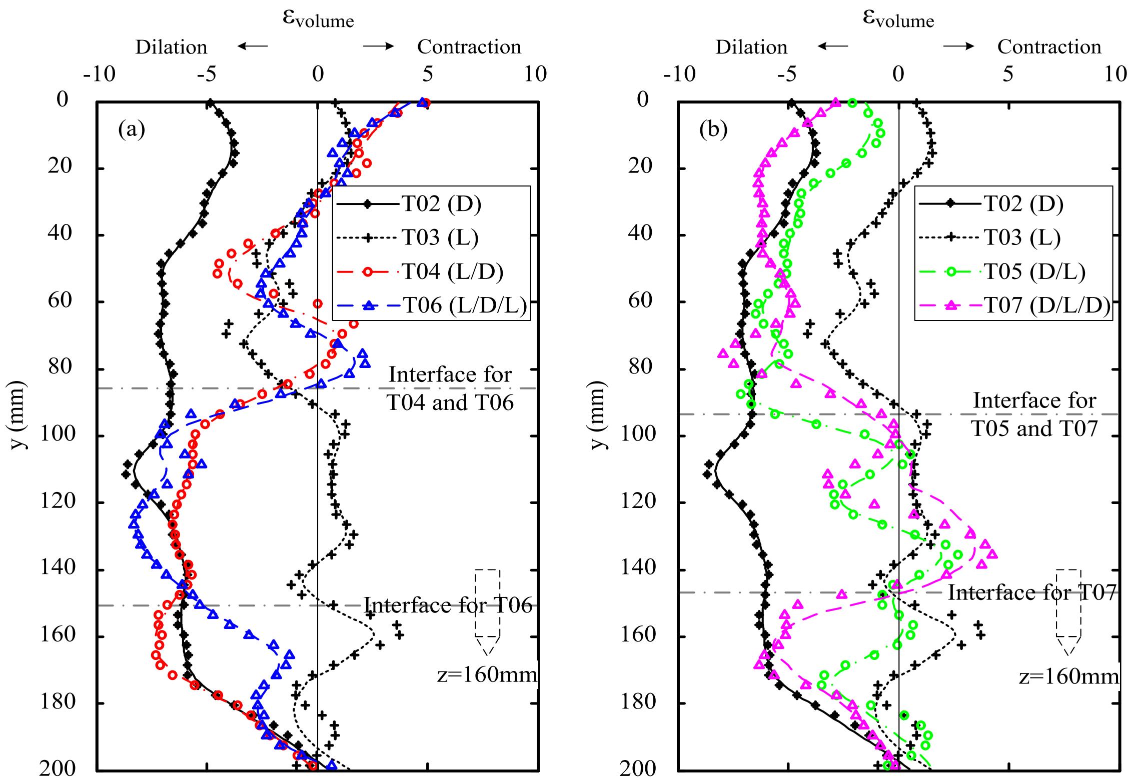

Fig. 16: Cumulative volumetric strain profiles for $2\,x/B = 2$ after $160\,mm$ of penetration: (a) T04 and T06; (b) T05 and T07

List of Tables

Table 1: Details of sample for each centrifuge test

Test ID	Soil Description	Depth of Soil 1 (mm)	Depth of Soil 2 (mm)	Depth of Soil 3 (mm)
T02	Uniform Dense (D)	301	-	-
T03	Uniform Loose (L)	298	-	-
T04	Loose over Dense (L/D)	85	205	-
T05	Dense over Loose (D/L)	97	201	-
T06	Thin Dense Layer (L/D/L)	87	65	142
T07	Thin Loose Layer (D/L/D)	90	57	153

Table 2: Properties of the Fraction E silica sand (Tan, 1990)

Property	Fraction E sand
Grain size d_{10} (mm)	0.095
Grain size d_{50} (mm)	0.14
Grain size d_{60} (mm)	0.15
Specific gravity G_s	2.65
Maximum void ratio (e_{max})	1.014
Minimum void ratio (e_{min})	0.613
Friction angle at constant volume (ϕ'_{cv})	32°